High Frequency Observations by GTM Antenna Range Beam Steering

Marco D'Errico, Antonio Moccia, and Sergio Vetrella

Faculty of Engineering, University of Naples "Federico II"
Piazzale V. Tecchio, 80 - 80125 Napoli (Italy)

ABSTRACT

The Global Topography Mission (GTM) is a proposed space mission for obtaining high resolution digital elevation models of the Earth surface by SAR (Synthetic Aperture Radar) interferometry and laser altimetry. This paper analyses the potential of GTM for natural disaster management. Since for most major types of disasters which are short-lived, the frequency of observation of normal satellite systems is a severe limitation, the authors propose the use of a SAR with a range steerable antenna. In this case, a significant increase in the observation frequency can be accomplished. In particular, the authors identify an orbit which points out the effectiveness of such a system for natural disaster relief. Moreover, an experimental application of GTM for natural disaster prevention and preparedness, based on differential interferometry techniques, is analysed in details. Two orbits which guarantee the observation of Vesuvius volcano every day for about two months are computed and a height difference error budget is derived. The measurement accuracy is of about 1 cm.

INTRODUCTION

Topographic information is vital for the land sciences, such as geology, geophysics, ecology, soil sciences, hydrology, botany, and glaciology (Topographic Science Working Group, 1988). Currently, topographic data are limited by coverage and accuracy, particularly at the more precise scales.

Interferometric SAR (INSAR) has been proposed and demonstrated as a successful topographic mapping technique (Zebker and Goldstein, 1986; Gabriel and Goldstein, 1988; Prati and Rocca, 1990) and many authors have analysed INSAR height accuracy (Li and Goldstein, 1990; Prati and Rocca, 1990; Moccia and Vetrella, 1992; Rodriguez and Martin, 1992; Zebker and Villasenor, 1992). INSAR offers high resolution DEMs (Digital Elevation Model) and is not affected by clouds, precipitation, and local time (radio frequencies allow night observations).

In order to achieve global, high resolution topographic coverage JPL (Jet Propulsion Laboratory) and NASA GSFC (Goddard Space Flight Center), Alenia Spazio and University of Naples (under NASA and ASI contract respectively) have been studying a new space mission: the Global Topography Mission (GTM). GTM configuration consists of two twin satellites orbiting on nearly parallel orbits and each carrying a laser altimeter (Bufton, 1989; Gardner, 1992; Harding *et al.*, 1993) and a SAR (Synthetic Aperture Radar). The SAR interferometry is achieved by one transmitting and two receiving antennae. An accurate estimate of antenna phase centre positions is achieved by differential GPS (Global Positioning System) and attitude control system. The possibility of using two laser sensors for real-time determination of the baseline between the two satellites is presently under study. Moreover, GTM will allow comparison between INSAR DEM and laser DEM.

The main goal of GTM, i.e. global topographic mapping, would be achieved in about three months, but additional scientific experiments are planned during the extended phase of the mission. In this context, it is worth studying INSAR applications to natural disaster management. In this area three main goals can be identified: preparedness, prevention, and relief. Preparedness consists of the minimisation of losses when a disaster strikes, in prevention one tries to avoid or control hazards, and in relief aid is provided after a disaster occurrence. As shown by Walter (1989), spaceborne remote sensing applications to disaster management are strongly limited by a trade-off between spatial and temporal resolution. Existing satellites achieve high temporal resolution by decreasing spatial resolution (e.g. meteorological satellites). On the other hand, due to orbital and data rate constraints, remote sensing satellites can accomplish high geometric resolution only at the expense of swath width and repetitivity.

INSAR offers a high resolution image and a DEM with an accuracy adequate for natural disaster mapping, while

prevention and preparedness can be carried out by a differential INSAR, which can measure altimetric changes at centimetric level (Gabriel *et al.*, 1989). Finally, the temporal resolution constraints could be overcome by the capability of antenna range beam steering.
This paper demonstrates that an INSAR with range steerable antennae can achieve both high temporal and high spatial resolution. Consequently, it is the only space instrument candidate for natural disaster management.

1. ANALYSIS OF TEMPORAL RESOLUTION

1.1 GTM main characteristics

The GTM will be on a nearly circular repetitive orbit, with a repetition factor of about 15 and a repetition period of about three months but less than 90 days. In order to guarantee global coverage in the repetition period, the distance between tracks must be smaller then the radar swath, which is about 35 Km at an altitude of about 560 Km (Kakuda, 1993).
The distance between the two satellites varies from 2 Km at the equator to 800 m at latitudes of ± 65°. Because of the baseline reduction with latitude, the INSAR works only in the range of latitude ± 65°. Topographic mapping of latitudes between 65° and 79° is obtained by modifying the orbit to obtain adequate baselines. Moreover, due to data rate restrictions, the INSAR and the laser altimeter operate during the ascending and descending phase respectively for the first three months of the mission. During the next three months, a second global topo data set is gathered by changing the operating phases of the two sensors. The acquisition of both ascending and descending INSAR data allows to overcome, or at least to reduce, geometrical distortion due to terrain morphology.
GTM antennae transmit in L-band (wavelength of 24 cm) with a bandwidth of 20 MHz, using a nominal off-nadir pointing angle of 30°. INSAR resolutions are 7.5 m (slant range) and 5.9 m (azimuth, 1 look).

1.2 Temporal resolution simulation

In order to study the temporal resolution of a steerable sensor, a model of the sensor-Earth relative motion was developed (D'Errico *et al.*, 1992). This model accounts for a varying off-nadir pointing angle, first order orbital perturbations, and target latitude.
The simulation was carried out for the orbits the parameters of which are listed in table 1. We analysed a set of sun-synchronous orbits with altitudes of about 560 Km, as selected in preliminary GTM studies (Kakuda, 1993). Of course we neglected the orbit 1245/83 because it corresponds to an integer repetition factor (15) which makes impossible high resolution global coverage. The repetition factor (Q=R/N) is expressed as the integer number of orbits (R) divided by the integer number of days (N) in the repetition period. The Earth surface was modelled by 100,000 randomly distributed points in the range of latitude ± 70°. We supposed the antenna beam steerable between 15° and 45° with respect to the nominal off-nadir angle (30°). The possibility of having off-nadir viewing angle on both sides of the spacecraft was neglected because of mechanical and electronical complexity. The temporal resolution was studied taking into account the following aspects: the time required for the first observation and the time interval between successive observations of each point. In the simulation we considered either cases of only ascending nodes or both ascending and descending nodes.
In order to study the former aspect, we determined the probability distribution of observation time. We present mean values and standard deviations of first observation time and the time required for the first observation of 95% points. This last parameter is necessary since standard deviations are quite large. The three parameters are plotted in figures 1 and 2, which put in evidence that the best orbit has a repetition factor of 1240/83 in both cases of either ascending nodes only or both ascending and descending nodes. In the figures, the x-axis time interval is equal to five days.
With reference to the latter aspect, we computed the probability distributions of the time interval between successive observations of the same point. Then, the mean values and the standard deviations of the time interval between observation i and $i-1$, and the mean values and the standard deviations of the time interval required to re-observe 95%

Table 1 - Main parameters of considered orbits.

Orbit Repetition Factor Q	Orbit Altitude h (Km)	Orbit Inclination i (°)	Nodal Period τ (s)	Equatorial Adjacent Track Distance (Km)
1240/83	579.67	97.714	5783.2	32.319
1241/83	575.93	97.699	5778.6	32.293
1242/83	572.18	97.684	5773.9	32.267
1243/83	568.45	97.670	5769.3	32.241
1244/83	564.72	97.655	5764.6	32.215
1246/83	557.27	97.627	5755.4	32.163
1247/83	553.55	97.612	5750.8	32.137
1248/83	549.84	97.598	5746.2	32.111

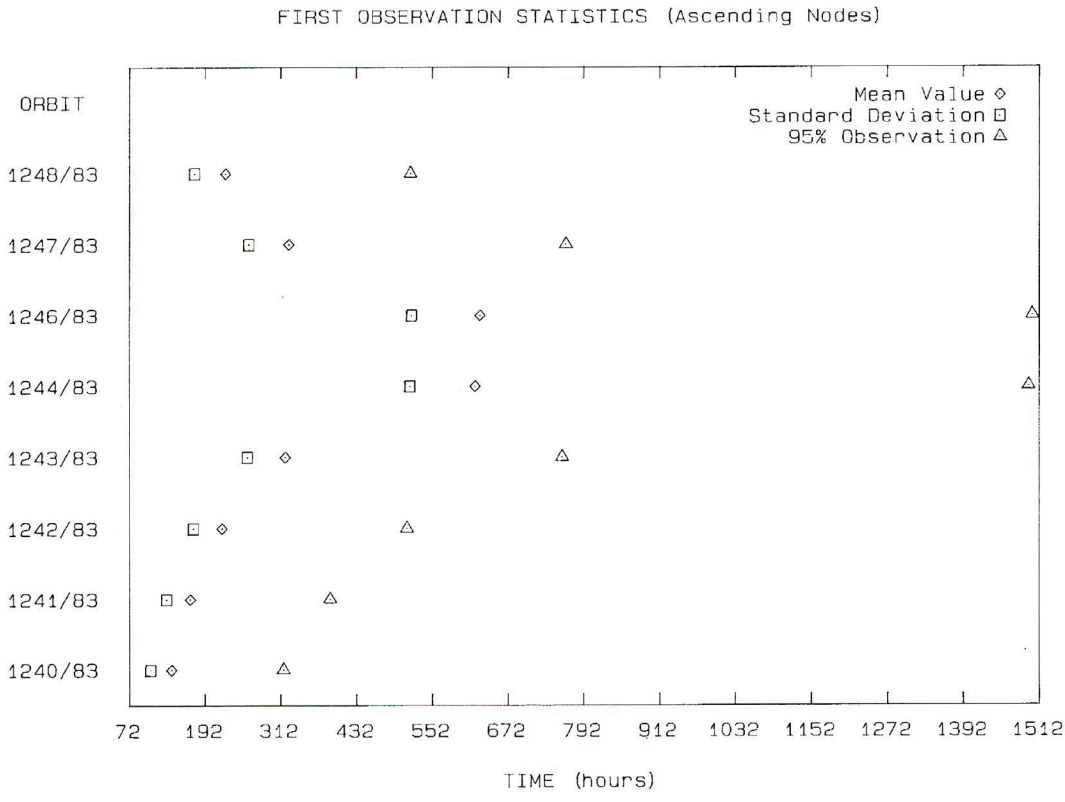

Fig. 1 - Mean value and standard deviation for the first observation of the target, and time required for the observation of 95% targets, for each selected orbit and considering ascending nodes only.

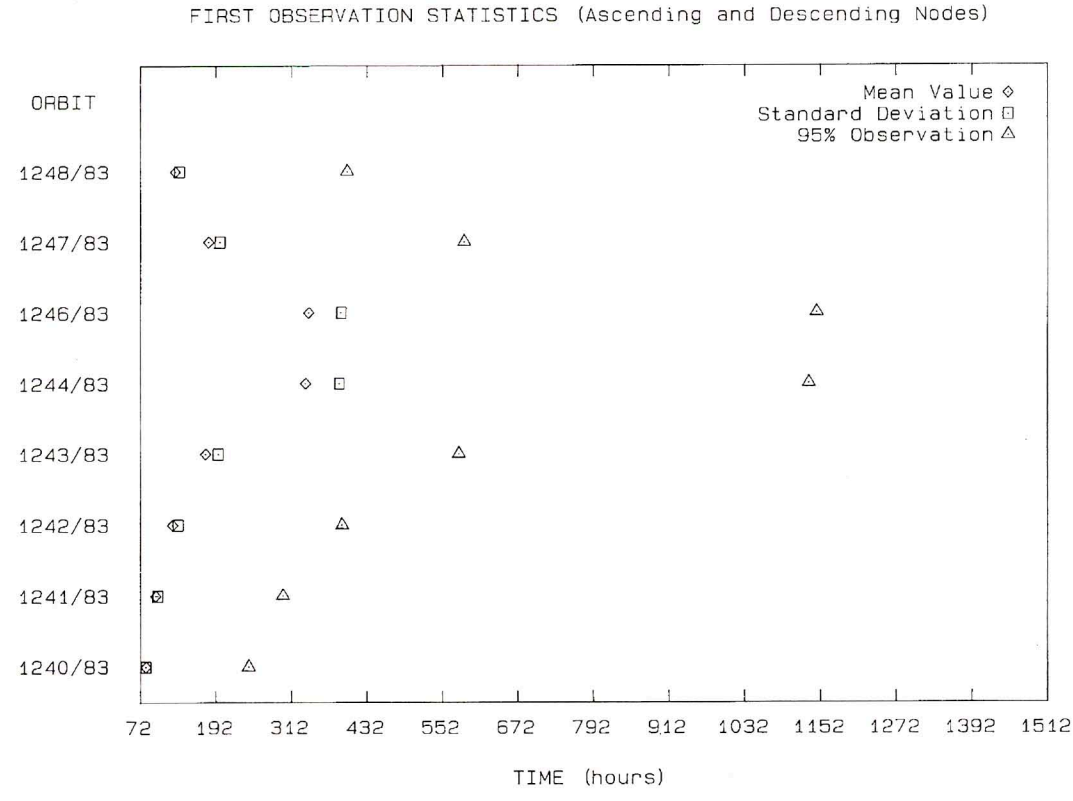

Fig. 2 - Mean value and standard deviation for the first observation of the target, and time required for the observation of 95% targets, for each selected orbit and considering both ascending and descending nodes.

points were computed. Again, the latter two values are necessary because of large values of standard deviations. Statistics were computed considering all the 100,000 points on the Earth surface and only the observations that cover 100% points in the repetition period, i.e. we considered the i-th observation only if all the randomly distributed points have been observed i-times. The number of considered observations is listed in table 2. The above four parameters are plotted in figures 3 and 4. These figures show a different trend with respect to the first aspect: now the best orbit is 1244/83, which performs the observation every 25.6 hours for 95% points in the case of ascending nodes only.

The above analysis points out a trade-off between the first observation time and the time interval between two successive observations: the orbit with the minimum delay of the first observation (1240/83) is one of the worst from the re-observation point of view, while the orbit with the best time intervals (1244/83) does not offer a satisfactory first observation time.

In order to gain further insight into these contrasting aspects, in figures 5, 6, 7, and 8 we plot the curves of relative cumulative frequencies of observation time. They refer to the observations listed in table 2 for the orbit 1240/83 and 1244/83. The orbit 1240/83 curves reach the 100% frequency sooner than the 1244/83 curves, but the latter have much more regular trend, in fact they are nearly parallel.

Table 2 - Maximum number of the observations of 100,000 targets, achieved in a repetition period, for the considered orbits.

Repetition Factor	Number of Observation of 100% Points in a Repetition Period	
	Ascending Nodes	Ascending and Descending Nodes
1240/83	14	28
1241/83	14	28
1242/83	14	28
1243/83	14	28
1244/83	13	26
1246/83	13	26
1247/83	13	26
1248/83	13	26

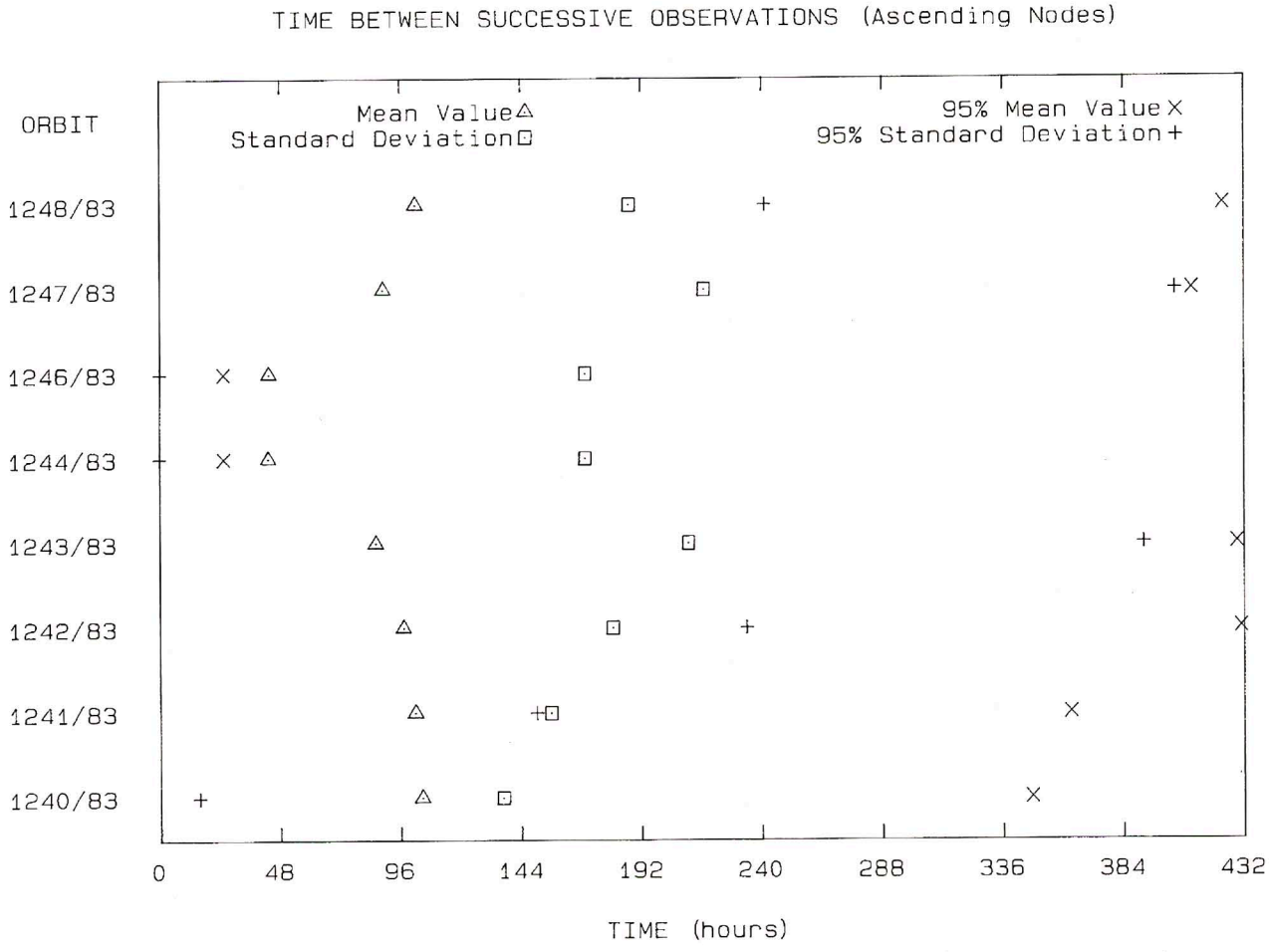

Fig. 3 - Mean value and standard deviation of time intervals for re-observation of the target, and mean value and standard deviation of time intervals for re-observation of 95% targets, for each selected orbit and considering ascending nodes only.

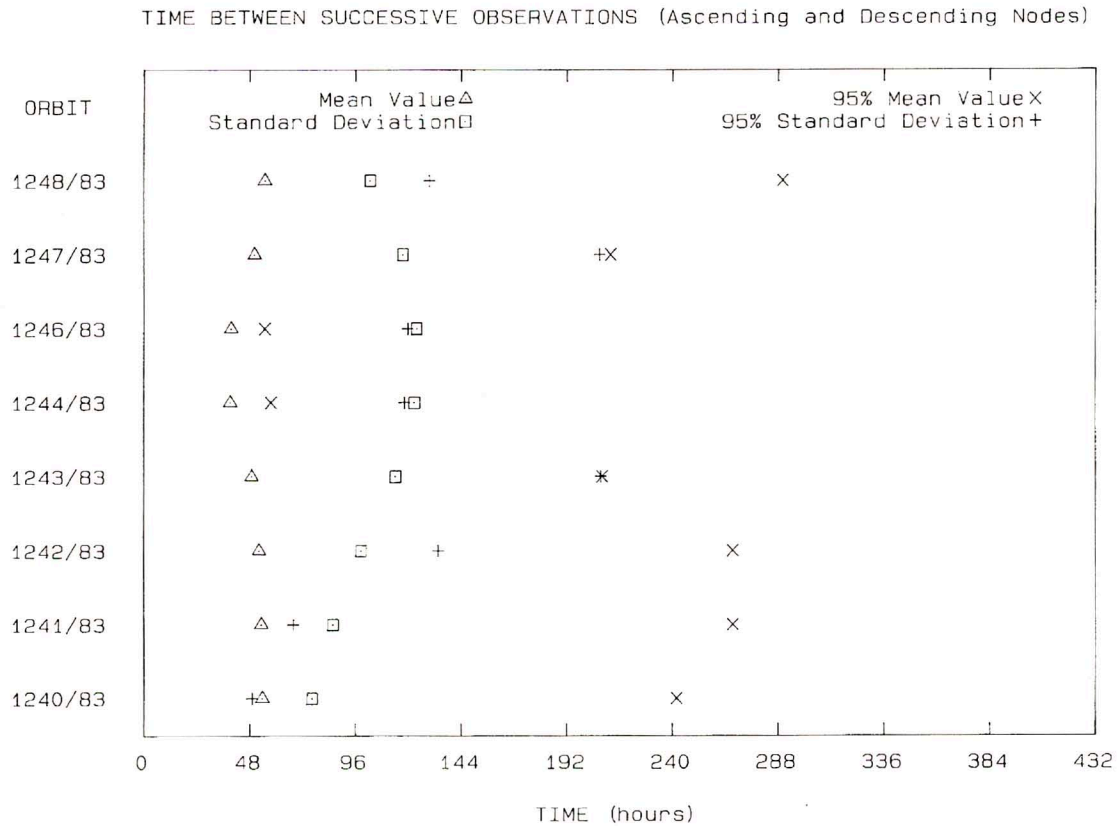

Fig. 4 - Mean value and standard deviation of time intervals for re-observation of the target, and mean value and standard deviation of time intervals for re-observation of 95% targets, for each selected orbit and considering both ascending and descending nodes.

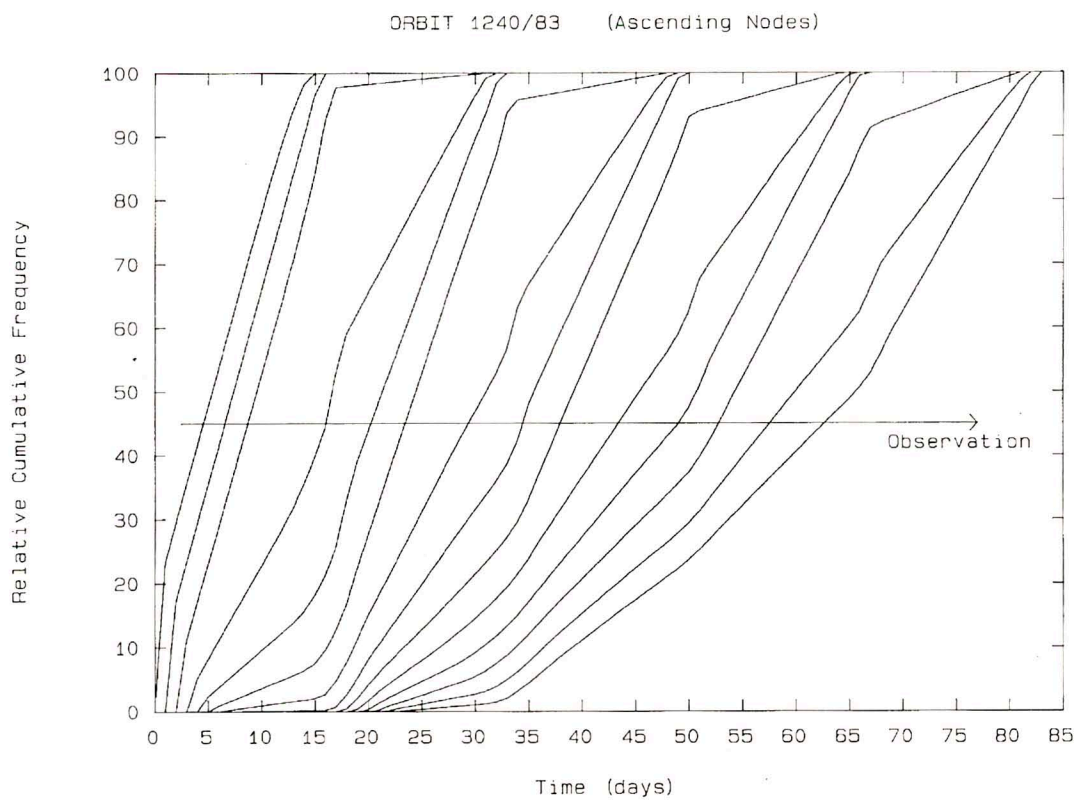

Fig. 5 - Relative cumulative frequency of observation time for the orbit 1240/83 considering ascending nodes only.

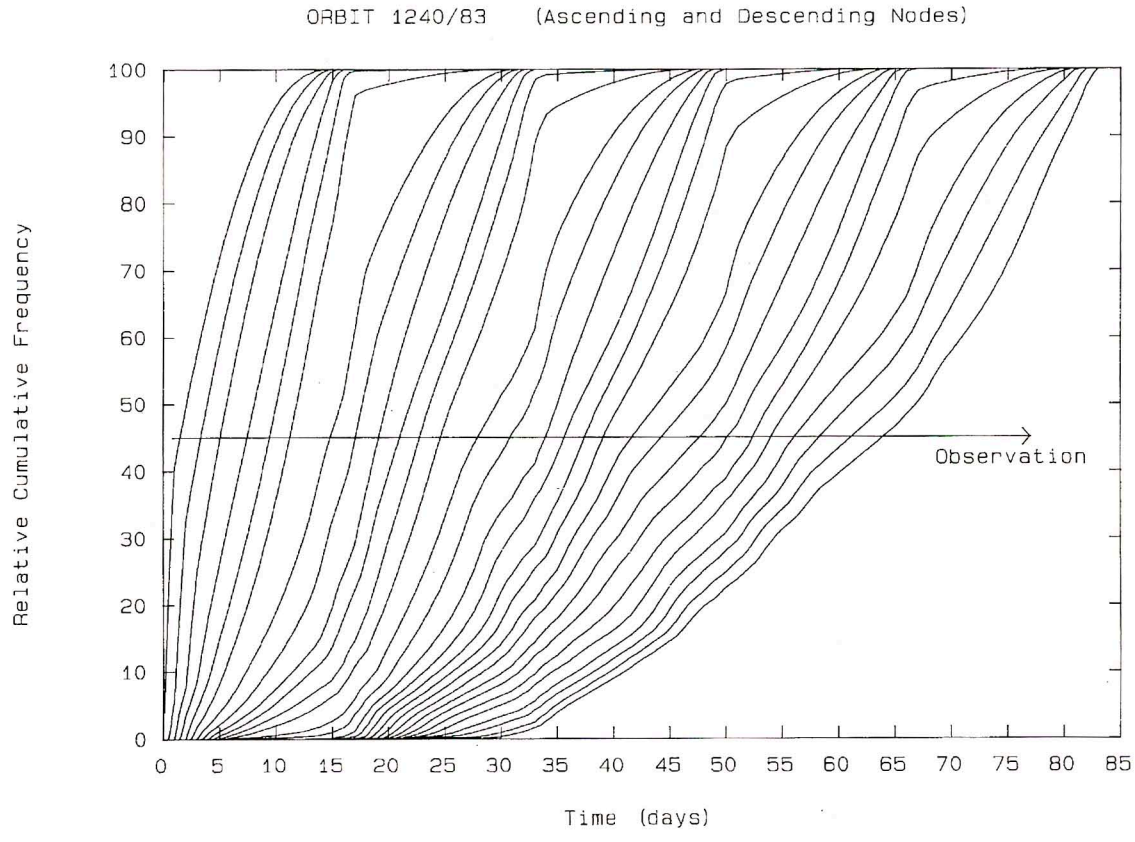

Fig. 6 - Relative cumulative frequency of observation time for the orbit 1240/83 considering both ascending and descending nodes.

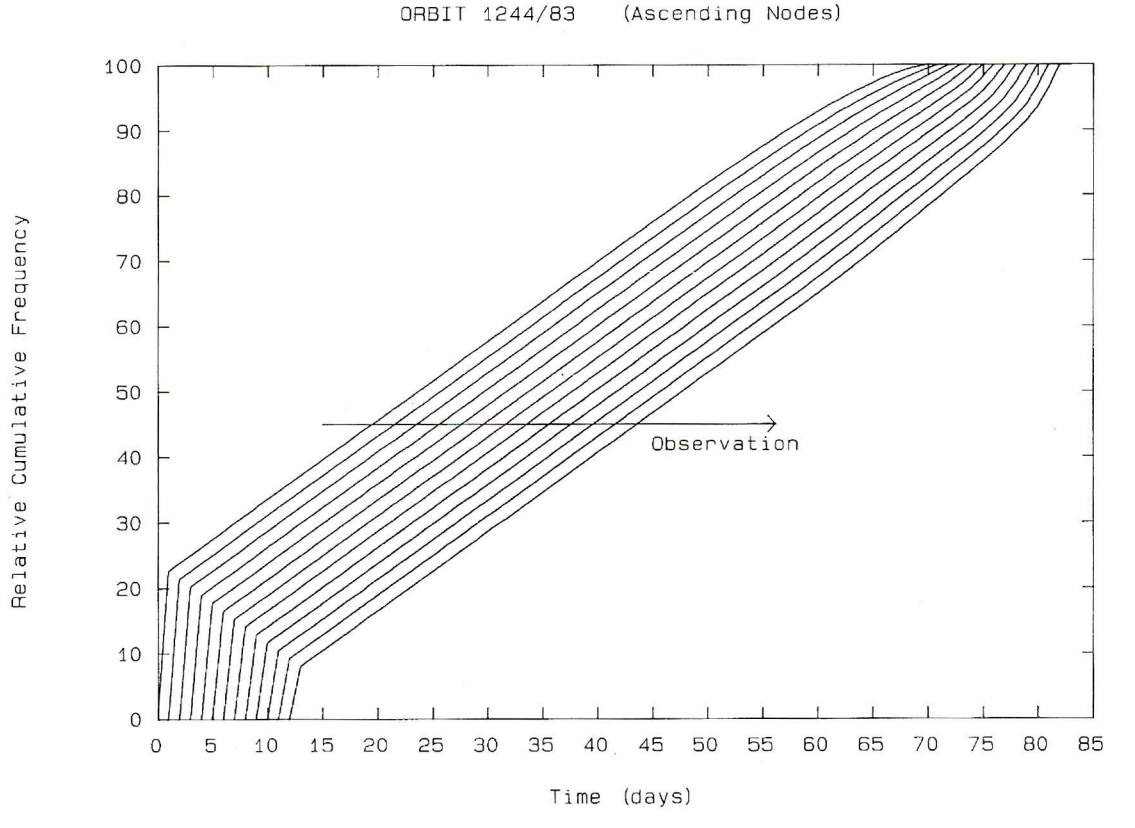

Fig. 7 - Relative cumulative frequency of observation time for the orbit 1244/83 considering ascending nodes only.

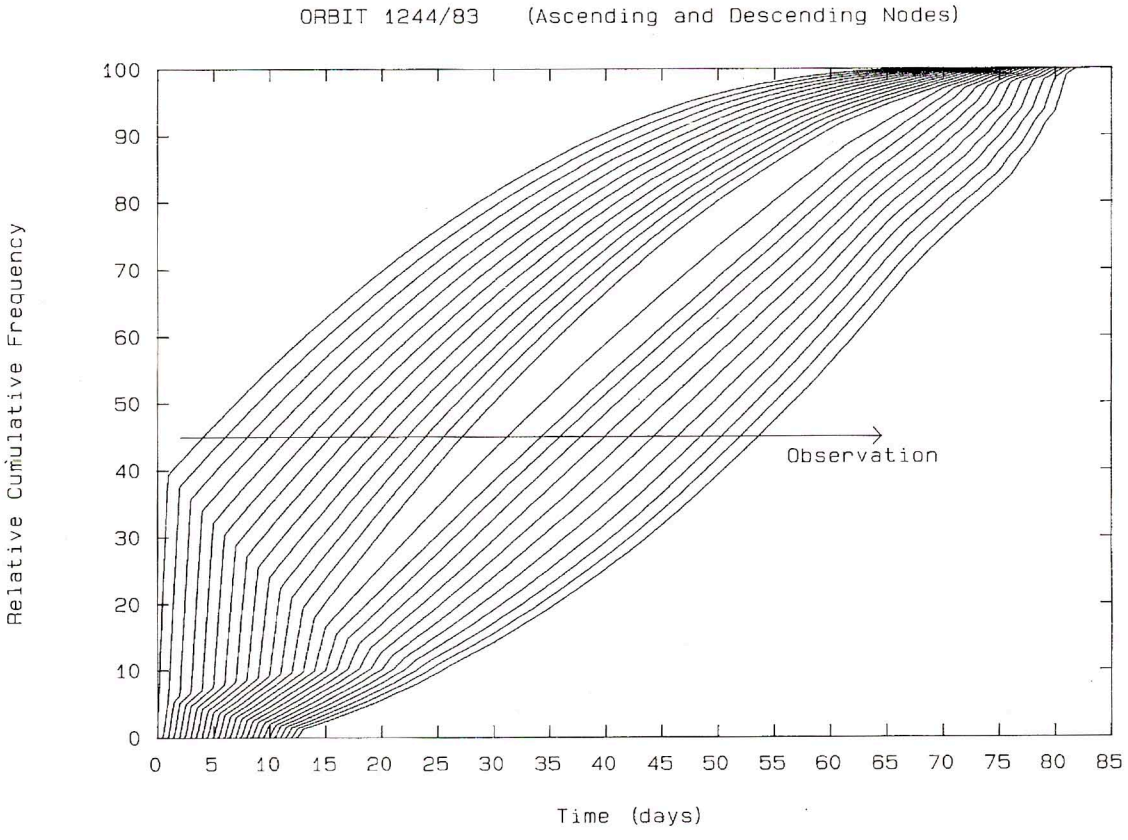

Fig. 8 - Relative cumulative frequency of observation time for the orbit 1244/83 considering both ascending and descending nodes.

In conclusion, we showed that it is possible to improve either the time required for the first observation or the time interval between successive observations. This result can be interpreted relating the repetition period to the swath pattern. Since a nearly integer repetition factor (such as 1244/83) gives adjacent ground tracks at successive times with a minimum orbital drift (Duck and King, 1983), the sensor swaths present large overlaps and, consequently, allow short re-observation times. On the other hand, an orbit with a larger drift (such as 1240/83) gives a shorter first observation time, because of the reduced swath overlaps.
As a quantitative result we identified two orbits which are slightly different in altitude (about 15 Km) and inclination (about .06°).

2. NATURAL DISASTER MANAGEMENT BY GTM

2.1 Relief

By choosing the orbit 1240/83, GTM will access 95% of the Earth surface in about 10 days by antenna range beam steering between 15° and 45°.
In this way if a natural disaster occurs during the nominal mission (first three months), GTM will produce both a DEM and a high resolution SAR image of the involved area. These data will allow a more effective intervention: identification of evacuation routes, sites of temporary dwellings, sources of water (Walter, 1989).
In this phase of the mission we will test the usefulness of GTM for natural disaster relief.

2.2. Prevention and preparedness

Natural disaster prevention and preparedness can take advantage of elevation change measurements at centimetric level in order to detect small crustal motions and volumetric changes which are premonitory events of floods, landslides, avalanches, volcanic eruptions, earthquakes, and so on. INSAR error budgets were proposed by several authors (Li and Goldstein, 1990; Rodriguez and Martin, 1992; Zebker and Villasenor, 1992) who demonstrated that INSAR DEMs can not achieve the required height accuracy. Whereas, differential INSAR allows an extreme reduction of the phase error impact on height difference measurements, as shown by Gabriel *et al.* (1989).
Differential interferometry measures elevation changes, instead of absolute heights, and needs three SAR images of

the same area. GTM achieves two contemporary SAR images during the first pass, whereas the third image is obtained by only one of the two antennae during the second pass. Consequently, it is not affected by ambiguity problem (Gabriel *et al.*, 1989). Moreover, if ascending and descending orbits are available for SAR interferometry, two components of the crustal motion can be derived.

The electronic range steering of antenna beam allows a frequent re-observation of selected test-sites and, then, a large number of measurements. In this case the best orbit must have a trend similar to that derived for the orbit 1244/83, i.e. with a short time delay between successive observations. Of course, an orbit with an adequate inter-track distance must be chosen to avoid images decorrelation (Prati and Rocca, 1990).

Assuming a flat Earth, a 2π phase shift occurs at a slant-range difference (Δr) which can be expressed as a function of the satellite altitude (h), the baseline (B_2), the wavelength (λ) and the off-nadir pointing angle (ϑ) as follows (figure 9):

$$\Delta r = \frac{\lambda h \sin\vartheta}{2B_2 \cos^3\vartheta} \tag{1}$$

Assuming Δr equal to n_r resolution elements, the maximum baseline ($B_{2\,max}$) is given by:

$$B_{2\,max} = \frac{\lambda h \Delta f \sin\vartheta}{c n_r \cos^2\vartheta} \tag{2}$$

where c is the light velocity and Δf is the chirp bandwidth.

The distance (s) between two satellite positions along adjacent orbits can be approximately expressed as a function of latitude (ϕ) as follows:

$$s = \frac{2\pi}{R}(R_\oplus + h)\cos\phi \tag{3}$$

where $R_\oplus$ is the Earth radius and R is the integer number of orbits in the repetition period.

Equations (2) and (3) allow to compute a repetitive orbit which has an inter-track distance adequate for interferometric applications. Of course, it is necessary to select an altitude as close as possible to the nominal one.

2.2.1 Vesuvius volcano experiment

As an example, we studied the feasibility of a crustal motion detection experiment considering an extended area on the Vesuvius volcano (40.82° North latitude, 14.38° East longitude). We identified two orbits the parameters of which are listed in table 3. These orbits allow one observation of the Vesuvius test site every day for a period of about 2 and 4 months, respectively. In particular we chose a period of ten days with 11 observations of the test site at a viewing angle of about 40° (from 39.981° to 41.587° for the orbit 9494/633 and from 39.995° to 40.932° for the orbit 16501/1100). The baseline is 3.68 Km for the former orbit, 1.94 Km for the latter. Since at a looking angle of 40° and assuming n_r=2, equation (2) yields a maximum allowable baseline of about 6.4 Km, the computed baselines are adequate for differential interferometry. Moreover, the deployment of arrays of corner reflectors in range direction allows an additional and significant improvement in the height difference measurements accuracy (Monti Guarnieri *et al.*, 1992).

It is worth noting that the two proposed orbits have a long repetition period which makes impossible their use during the nominal phase of the mission. Consequently, this experiment could be conducted for a limited number of selected test sites during the extended phase of the mission.

Table 3 - Main parameters of the orbits proposed for the differential interferometry experiment.

Orbit Repetition Factor Q	Orbit Altitude h (Km)	Orbit Inclination i (°)	Baseline B_2 (Km)	Re-Observation Time (Hour)	Observation Period (Months)
9494/633	561.48	97.643	3.675	24	2
16501/1100	560.71	97.640	1.941	24	4

3. GTM DIFFERENTIAL INTERFEROMETRY ERROR BUDGET

In this section we present an error budget of GTM differential INSAR for point targets. The point target assumption allows to obtain results which are useful for evaluating the system impulse response and are appropriate to analyse the performance of the radar when viewing man-made targets (calibration). We will also assume that systematic errors have been essentially removed by some small set of ground control points, so we will consider only random errors caused by noise and geometric uncertainties.

The first two SAR images are acquired contemporaneously during the first passage on the test site, while the third SAR image is obtained by one antenna during the second passage. We refer to the slant ranges as R_1, R_2, R_3, and to the baselines between the passages 1 and 2, and 1 and 3 as B_1 and B_2 respectively (figure 9). The off-nadir looking angle of the first image is ϑ. Let us suppose that the pixel height during the first passage (images 1 and 2) is z and it increases until a value $z + \Delta z$ before the second passage (image 3).

Considering that the first and the third antenna transmit and receive the signal, while the second antenna receives the

signal transmitted by the first antenna, the phases of the three SAR images can be computed as follows:

$$\phi_1 = \frac{2\pi}{\lambda} 2R_1 \tag{4}$$

$$\phi_2 = \frac{2\pi}{\lambda} (R_1 + R_2) \tag{5}$$

$$\phi_3 = \frac{2\pi}{\lambda} 2R_3 \tag{6}$$

Assuming flat Earth and constant satellite altitude, the slant ranges R_2 and R_3 can be expresses as function of R_1, ϑ, B_1, B_2:

$$R_2 = \left[(h - z)^2 + (R_1 \sin\vartheta - B_1)^2 \right]^{1/2} \cong R_1 - B_1 \sin\vartheta + \frac{B_1^2}{2R_1} \tag{7}$$

$$R_3 = \left[(h - z\,\Delta z)^2 + (R_1 \sin\vartheta - B_2)^2 \right]^{1/2} \cong R_1 - B_2 \sin\vartheta + + \frac{B_2^2}{2R_1} - \Delta z \cos\vartheta \tag{8}$$

Introducing a differential phase (Φ) as:

$$\Phi = \frac{B_1}{2B_2} \Delta\phi_{13} - \Delta\phi_{12} \tag{9}$$

we obtain:

$$\Delta z = \frac{B_2}{B_1} \frac{\lambda}{2\pi \cos\vartheta} \Phi + \frac{B_2^2 - B_1 B_2}{2R_1 \cos\vartheta} \tag{10}$$

Assuming incorrelated parameters (Li and Goldstein, 1990) and differentiating equation (10) the height difference uncertainties ($\sigma_{\Delta z}^{(i)}$, $i = 1,2,3$) are evaluated:

$$\sigma_{\Delta z}^{(1)} = \frac{B_2}{B_1} \frac{\lambda}{2\pi \cos\vartheta} \sigma_\Phi \tag{11a}$$

$$\sigma_{\Delta z}^{(2)} = \left(\Delta z + \frac{B_2^2}{2R_1 \cos\vartheta} \right) \frac{\sigma_{B_2}}{B_2} \tag{11b}$$

$$\sigma_{\Delta z}^{(3)} = \left(\frac{B_2^2 - 2B_2 B_1}{2R_1 \cos\vartheta} - \Delta z \right) \frac{\sigma_{B_1}}{B_1} \tag{11c}$$

where σ_Φ, σ_{B1}, and σ_{B2} are the uncertainties in the differential phase and baselines. Assuming large Signal to Noise Ratio (SNR) and Rician statistics on the received phasors (Goodman, 1975), we get:

$$\sigma_\Phi = \frac{\sqrt{1 + \left(\frac{B_1}{2B_2} \right)^2}}{SNR} \tag{12}$$

Since the GTM baseline will be known with centimetric accuracy ($\sigma_{B1} = \sigma_{B2} = 3cm$ and assuming SNR=19.5dB (using large corner reflectors this value could be easily increased), equations (11a), (11b), (11c), and (12) yield a centimetric error in the height difference measurements, which is shown in table 4 for the two selected orbits.

Table 4 - Differential interferometry error budget for the two selected orbits.

Error	Repetition Factor	
	9494/633	16501/1100
σ_Φ (°)	6.196	6.514
$\sigma_{\Delta z}^{(1)}$ (cm)	1.309	7.270×10^{-1}
$\sigma_{\Delta z}^{(2)}$ (cm)	1.00×10^{-2}	5.563×10^{-3}
$\sigma_{\Delta z}^{(3)}$ (cm)	3.727×10^{-3}	6.182×10^{-3}
$\sigma_{\Delta z}^{TOT}$ (cm)	1.309	7.270×10^{-1}

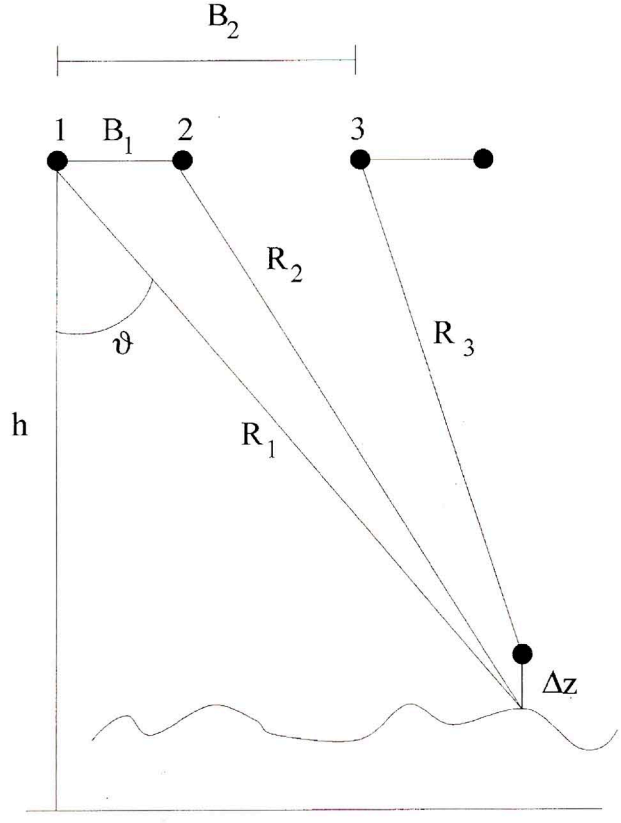

Fig. 9 - Geometry of GTM differential interferometry.

CONCLUSIONS

In this paper the potentiality of GTM for natural disaster management was analysed. We demonstrated that the existing main limitation of spaceborne high resolution sensors (i.e. temporal resolution) can be largely overcome by using a pointing antenna.

We then identified an orbit which can offer an adequate temporal resolution for natural disaster mapping. This orbit is very close to the nominal one and can be achieved by a slight modification of satellite altitude and inclination.

We also analysed the application of GTM for natural disaster prevention and preparedness, by using differential interferometry techniques. In order to achievé an adequate interferometric baseline, small changes in orbit altitude and inclination are required, but they imply a significant increase of the repetition period, which also causes a large average time to obtain the first data set. To test the utility of this configuration, we analysed the feasibility of a crustal motion detection experiment on an extended test site at the latitude of the Vesuvius volcano (40.82° North). It is worth noting that the orbit adequate for the proposed experiment of differential interferometry does not guarantee global coverage requirements of GTM, then the proposed experiment must be carried out during the extended phase of the mission.

In conclusion, we proved that GTM can be an effective space system for natural disaster relief. In fact, the antenna range beam steering allows a remarkable and global improvement in observation repetitivity. In addition, GTM differential interferometry can allow natural disaster prevention and preparedness experiments. GTM could become operational from this point of view considering a third satellite flying behind the proposed twin satellites with an adequate time delay and with the same capability of antenna range beam steering. In this case the third image required for differential interferometry is obtained by the third satellite and the stringent requirement on the orbital inter-track distance disappears. Depending on the third satellite ascending node, it is possible to select a baseline which improves significantly the height difference measurements accuracy.

REFERENCES

Bufton, J.L., 1989. Laser altimetry measurements from aircraft and spacecraft. *Proceedings of the IEEE*, Vol. 77, No. 3, pp. 463-477.

D'Errico M., A. Moccia, and S. Vetrella, 1992. High Frequency Observation of Natural Disasters by SAR Interferometry. Accepted for publication by *Photogrammetric Engineering and Remote Sensing*.

Duck, K.I., and J.C. King, 1983. Orbital Mechanics for remote Sensing, Chapter 16 in Manual of Remote Sensing (2nd ed.) (R.N. Colwell, ed.), American Society of Photogrammetry, Falls Church, Virginia, Vol. 1, pp. 704.

Gabriel, A.K., and R.M. Goldstein, 1988. Crossed orbit interferometry: theory and experimental results form SIR-B. *International Journal of Remote Sensing*, Vol. 9, No. 8, pp. 857-872.

Gabriel, A.K., R.M. Goldstein, and H.A. Zebker, 1989. Mapping small elevation changes over large areas: differential radar interferometry. *Journal of Geophysical Research*, Vol. 94, No. B7, pp 9183-9191.

Gardner, C.S., 1992. Ranging Performance of Satellite Laser Altimeters. *IEEE Transaction on Geoscience and Remote Sensing*, Vol. 30, No. 5, pp. 1061-1072.

Goodman, J.W., 1975. Statistical properties of laser speckle patterns, in Dainty J.C., Ed., Laser Speckle and Related Phenomena, New-York: Springler-Verlag.

Harding, D.J., J.L. Bufton, and J.J. Frawley, 1993. Satellite Laser Altimetry of Terrestrial Topography: Vertical Accuracy as a Function of Surface Slope, Roughness, and Cloud Cover. Submitted to *IEEE Transaction on Geoscience and Remote Sensing*.

Kakuda, R., 1993. Dual Satellite Mission Overview. Presented at TOPSAT JPL/Italy Joint Study, Pasadena, 22 March 1993.

Li, K., and R.M. Goldstein, 1990. Studies of Multibaseline Spaceborne Interferometric Synthetic Aperture Radar. *IEEE Transaction on Geoscience and Remote Sensing*, Vol. 28, No. 1, pp. 88-97.

Moccia, A., and S. Vetrella, 1992. A Tethered Interferometric Synthetic Aperture Radar (SAR) for a Topographic Mission. *IEEE Transactions on Geoscience and Remote Sensing*, Vol. 30, No.1, pp. 103-109.

Monti Guarnieri A., F. Parizzi, P. Pasquali, C. Prati, and F. Rocca, 1992. Developments in ERS-1 SAR Interferometry. *Proceedings. of 1st Workshop ERS-1 Fringe Working Group, ESA ESRIN*, Frascati, Italy, pp. 16.

Prati C., and F. Rocca, 1990. Limits to the resolution of elevation maps from stereo SAR images. *International Journal of Remote Sensing*, Vol. 11, No. 12, pp. 2215-2235.

Rodriguez, E., and J.M. Martin, 1992. Theory and design of interferometric synthetic aperture radars. *IEE Proceedings-F*, Vol. 139, No. 2, pp. 147-159.

Topographic Science Working Group, 1988. Topographic Science Working Group Report to the Land Processing Branch, Earth Science and Application Division, NASA Headquarters. Lunar and Planetary Institute, Houston, pp. 64.

Walter, L.S., 1989. Application of Satellite Technology to Disaster Management. In *Communication When it's Needed Most*, The Anneberg Washington Program in Communications Policy Studies of Northwestern University, David Webster ed., pp. 74-93.

Zebker, H.A., and R.M. Goldstein, 1986. Topographic Mapping From Interferometric Synthetic Aperture Radar Observations. *Journal of Geophysical Research*, Vol. 91, No. B5, pp. 4993-4999.

Zebker, H.A., and J. Villasenor, 1992. Decorrelation in Interferometric Radar Echoes. *IEEE Transactions on Geoscience and Remote Sensing*, Vol. 30, No. 5, pp. 950-959.